Int. J. Heat Mass Transfer. Vol. 29, No. 5, pp. 725–739, 1986
Printed in Great Britain

0017–9310/86 $3.00 + 0.00
Pergamon Journals Ltd.

Natural convection in narrow-gap, spherical annuli

J. L. WRIGHT* and R. W. DOUGLASS†

Department of Mechanical Engineering, 255 Walter Scott Engineering Center, University of Nebraska—Lincoln, Lincoln, NB 68588–0525, U.S.A.

(*Received* 19 *August* 1985 *and in final form* 11 *November* 1985)

Abstract—The subject of this paper is natural convection of fluid contained within narrow-gap, spherical annuli. The flows are presumed to be steady and the fluid is assumed to follow the Oberbeck–Boussinesq model. With the gap being very small relative to the outer sphere's radius, the dependent variables are solved for by using a regular perturbation method in powers of the relative gap width, ε. Solutions were found for a heated outer sphere through terms of order ε^{11}. The results include Nusselt numbers, and contours of streamlines and isotherms as functions of the Grashof and Prandtl numbers, ε, and Q, the dimensionless uniform energy generation rate parameter. The value of ε ranged from 0.1 to 0.001, Pr from 0.01 to 10, and Gr from 7×10^6 to 5×10^{12}.

1. INTRODUCTION

NATURAL convection flows in spherical annuli have been studied extensively for over 35 years. Most of the data obtained has been for wider gap cases. Presented here are results specifically addressing flows within narrow-gap annuli. The method used to compute the flow field takes advantage of the narrowness of the gap in that a regular perturbation method is used, expanding the dependent variables in powers of the small parameter ε, the dimensionless (or relative) gap width. This produces algebraic functions for the steady flow field which depend on the spatial coordinates and have the Grashof (or Rayleigh) number, the Prandtl number, and ε as parameters. In some cases, Q, the dimensionless energy generation rate is also a parameter.

Such a problem was posed as a first step in understanding the curious behavior of the flow field as first described in the flow visualization experiments of Bishop using air [1, 2], and later by Yin using water [3, 4]. A summary of these and other related flows is given by Powe *et al.* [5, 6]. As a brief outline of the phenomenon, consider that the fluid and (large gap) geometry are fixed so that the Grashof number is the sole characteristic variable for the annular flow field. Changes in it, then, can be thought of as changes in the temperature difference between the boundaries, the driving potential for the natural flow. If the temperature difference is 'small', the flow lines are found to be of a persistent, steady shape. For somewhat larger differences the flow may distort, but is still steady. Should the temperature difference exceed a critical value, the steady flows transform to a variety of unsteady, multiple eddy flows. Refer to Figs. 3 and 7 of Powe *et al.* [6] for documentation. The critical temperature difference, or Grashof number, for this transition is a function of the Prandtl number and ε tending, for a given Prandtl number, to decrease as ε approaches zero. It is our hypothesis that this sort of transition phenomenon is a bifurcation of the steady base flow due to an instability. The availability of a functional form of solution, as opposed to a tabular one, for the narrow-gap flows simplifies the study of the linear stability of the flow field. The stability computations are, however, not trivial. Aside from this specific problem area, the flow field of its own is of interest as an area of research.

It is the intent of this paper to present algebraic, functional solutions for the steady natural convection flows in the annulus formed by two concentric spheres whose radii are nearly identical. Their boundaries have uniform temperature with the inner sphere being cooled. The study of the influence of uniform energy generation on the solutions is also provided for. It is noted that the experimental parameters now available exceed the range of applicability of the present results.

First, the problem is formulated and the solution method is outlined. A discussion of the solutions and their range of applicability regarding parameter values is presented. A discussion of the results begins with the Nusselt number data and continues with the effect of the Grashof number (or Rayleigh number), the Prandtl number, the relative gap width, ε, and finally internal energy sources on the flow field. Lastly, brief closing comments are presented.

2. MODELLING THE FLOWS

Consider two spheres with common centers whose inner radius is R_i and outer radius is R_o. The gap width, L, is $R_o - R_i$ and the radius ratio is $\eta = R_i/R_o$. The relative gap width is then defined as

$$\varepsilon \equiv L/R_o = 1 - \eta. \quad (1)$$

* Currently, Mechanical Design Engineer, Texas Instruments, Inc., Lewisville, TX 75067, U.S.A.
† To whom correspondence should be addressed.

NOMENCLATURE

$\nabla^2( )$ Laplacian operator in spherical coordinates
$D^2( )$ $= \varepsilon^{-2}\partial^2/\partial\zeta^2 + [\varepsilon(\zeta-1)+1]^{-2} \times [\partial^2/\theta^2 - \cot\theta\,\partial/\partial\theta]$
$D^4( )$ $= D^2[D^2( )]$
g_0 gravitational acceleration constant [m s^{-2}]
Gr Grashof number, $g_0\beta\Delta T R_o^3/\nu^2$
Gr' modified Grashof number, $Gr\,\varepsilon^4/\sqrt{1-\varepsilon}$
$J(a, b)$ Jacobian operator, $a_\zeta b_\theta - a_\theta b_\zeta$
k thermal conductivity of the fluid [W m^{-1} °C^{-1}]
L gap width between spherical boundaries, $R_o - R_i$ [m]
$\overline{Nu}$ surface-averaged Nusselt number, cf. equation (27)
Pr Prandtl number, ν/α
q local heat flux, cf. equation (23)
$\dot{Q}$ volumetric energy generation constant [W m^{-3}]
Q dimensionless generation rate constant, $\dot{Q}R_o^2/k\Delta T$
r radial coordinate [m]
R_i, R_o inner and outer radius of the boundaries [m]
Ra the Rayleigh number, $Gr\,Pr$
Ra' modified Rayleigh number, $Ra\,\varepsilon^4/\sqrt{1-\varepsilon}$
$T(r, \theta)$ the temperature function [°C]
T_i, T_o inner and outer boundary temperatures [°C]
ΔT $= T_o - T_i$
v_r radial velocity component, $r^{-2}\,\mathrm{cosec}\,\theta\,\partial\psi/\partial\theta$ [m s^{-1}]
v_θ latitudinal velocity component, $-r^{-1}\,\mathrm{cosec}\,\theta\,\partial\psi/\partial r$ [m s^{-1}].

Greek symbols

α fluid thermal diffusivity [m^2 s^{-1}]
β fluid coefficient of thermal expansion [°C^{-1}]
δ_{ij} $= 1$ if $i = j$ or 0 if $i \neq j$
ε relative gap width, L/R_o
ζ stretched radial coordinate, $(r-\eta)/\varepsilon$
η radius ratio, R_i/R_o
θ latitudinal coordinate
ν fluid kinematic viscosity [m^2 s^{-1}]
ϕ longitudinal coordinate
$\psi(r, \theta)$ streamfunction [m^3 s^{-1}].

Superscripts

* physical or dimensional variable.

Subscripts

c critical value
lim limiting value
ζ $= \partial/\partial\zeta$
θ $= \partial/\partial\theta$.

The spheres will have a relatively narrow gap when $\eta \to 1$ or $\varepsilon \to 0$.

It is assumed that the flow has evolved to a steady state due to the naturally occurring buoyancy forces within the fluid arising from the local density variations due, in turn, to local temperature differences associated with $(T_o - T_i)$, the difference in boundary temperatures. Gravitational acceleration is presumed to be uniformly parallel and vertical as compared with a radial vector found on a planet or star. The fluid is assumed to follow the Oberbeck–Boussinesq approximation [7]. Finally, due to the presumed symmetry of the flows about the vertical axis passing through the spheres' centers, the flow field is independent of the longitudinal coordinate, ϕ, leaving r and θ as the independent spatial variables of the problem.

These assumptions allow a streamfunction, $\psi(r, \theta)$, to be used as a dependent variable and ultimately to have the pressure field eliminated as a variable. Thus the streamfunction, ψ, and the temperature are the dependent variables of the problem. In order to express the govening momentum and energy balance in terms of the relative gap width, ε, the transformation from the radial coordinate to the new coordinate, ζ, given by

$$\zeta = (r-\eta)/(1-\eta) = (r+\varepsilon-1)/\varepsilon \tag{2}$$

is used so that the domain shifts from $\eta \leqslant r \leqslant 1$ to $0 \leqslant \zeta \leqslant 1$ and of course the θ-range, $0 \leqslant \theta \leqslant \pi$ remains unaltered. In terms of ζ and θ then, the momentum and energy balance are

$$D^4\psi = \sqrt{Gr}\,\varepsilon^{-1}[\varepsilon(\zeta-1)+1]^{-2}\{2\,\mathrm{cosec}^2\,\theta D^2\psi \times J(\psi, [\varepsilon(\zeta-1)+1]\sin\theta) + \mathrm{cosec}\,\theta J(D^2\psi, \psi) - \sin\theta[\varepsilon(\zeta-1)+1]^2 J([\varepsilon(\zeta-1)+1]\cos\theta, T)\}, \tag{3}$$

and

$$\nabla^2 T = \sqrt{Gr}\,Pr\,\varepsilon^{-1}[\varepsilon(\zeta-1)+1]^{-2}\mathrm{cosec}\,\theta J(T, \psi) - Q, \tag{4}$$

wherein the variables are scaled as

$$r = r^*/R_o, \qquad \psi = \psi^*/\sqrt{g_0\beta\Delta T R_o^5}, \tag{5}$$

and

$$T = (T^* - T_i)/\Delta T.$$

The dimensionless parameters are

$$Q = \dot{Q}R_o^2/k\Delta T = \text{dimensionless energy generation rate},$$
$$Gr = g_0\beta\Delta T R_o^3/\nu^2 = \text{Grashof number}, \tag{6}$$

and

$$Pr = \nu/\alpha = \text{Prandtl number.}$$

The conditions to be satisfied by the solutions are first for the streamfunction:

$$\psi_\zeta(0, \theta) = \psi_\theta(0, \theta) = \psi_\zeta(1, \theta) = \psi_\theta(1, \theta) = 0$$
$$\psi_\zeta(\zeta, 0) = \psi_\zeta(\zeta, \pi) = 0 \tag{7}$$
$$\psi(0, \theta) = \psi(1, \theta) = 0$$

and for the temperature function:

$$T(0, \theta) = 0$$
$$T(1, \theta) = 1 \tag{8}$$
$$T_\theta(\zeta, 0) = T_\theta(\zeta, \pi) = 0.$$

3. SOLUTION METHOD AND PARAMETER VALUES

In this section, details regarding the method used to solve for ψ, $T = \psi$, $T(\zeta, \theta)$ are presented along with the solutions themselves. Since the dependent variables are implicitly dependent also on the Rayleigh (or Grashof) and Prandtl numbers, ε, and Q, it is necessary to estimate over which values of these parameters the solutions might be evaluated with the expectation that the solutions then predict the associated physical flow. This topic closes the section.

3.1. *The regular perturbation method*

The governing equations (3) and (4) along with conditions (7) and (8) lend themselves to a regular perturbation technique in terms of the small parameter, ε. Let

$$T(\zeta, \theta) - \sum_{m=0}^{M} \varepsilon^m T_m(\zeta, \theta),$$

and (9)

$$\psi(\zeta, \theta) = \sum_{n=0}^{N} \varepsilon^n \psi_n(\zeta, \theta),$$

so that the functions T_m and ψ_n can be solved in a step-by-step way. The series (9) are substituted into equations (3), (4), (7), and (8). In addition, (3) is multiplied by $\varepsilon^4[\varepsilon(\zeta-1)+1]^5$ and (4) by $\varepsilon^2[\varepsilon(\zeta-1)+1]^2$ to eliminate factors of ε in the denominators of the terms in the equations, noting that here ε is small and the case $\varepsilon = 0$ is a valid limit which occurs naturally in this problem. The effect of very small ε is therefore retained. Following these steps, all terms multiplied by like powers of ε are collected and individually set to zero. This produces partial differential equations for the 'nth' order function ψ_n and 'mth' order function T_m. These equations are shown in the Appendix. The boundary conditions for these problems are

$$\psi_n(0, \theta) = \psi_n(1, \theta) = (\psi_n)_\zeta(0, \theta) = (\psi_n)_\zeta(1, \theta) = 0, \quad n = 0, 1, 2, \ldots, N \tag{10}$$

and

$$T_m(0, \theta) = 0$$
$$T_m(1, \theta) = \delta_{mo}, \quad m = 0, 1, 2, \ldots, M.$$

As an example, the governing differential equations for the zeroth-order problem are:

$$\partial^4\psi_o/\partial\zeta^4 = 0,$$

and (11)

$$\partial^2 T_o/\partial\zeta^2 = 0$$

subject to (10) above. The solutions are:

$$\psi_o(\zeta, \theta) = 0$$

and (12)

$$T_o(\zeta, \theta) = \zeta.$$

3.2. *Higher-order solutions*

The solutions for higher-order functions depend upon lower-order solutions so that ψ_1, T_1 depend on ψ_o, T_o; ψ_2, T_2 on both ψ_1, T_1 and ψ_o, T_o, etc. Since T_o and ψ_o are known explicitly, then ψ_1, and T_1 can be found. Thus, this step-by-step approach allows solutions in exact, algebraic functional form to be obtained for virtually any order solution, in principle. In practice, the algebra, if done by hand, becomes extremely tedious. However, the computer is available to somewhat ease this limitation.

The solutions themselves, for a given order, can be grouped into polynomials in ζ multiplied by functions of θ, with appropriate factors of Grashof and Prandtl numbers, ε, and Q interspersed. Each power of ζ has an associated coefficient. These coefficients for terms through $M = N = 8$ have been found in exact form by Wright [8] and in that same work through $M = N = 11$ via computer generation. (N.B. A copy of ref. [8] may be obtained from R. W. Douglass for the cost of its reproduction.)

To illustrate the form of the solution, the expressions for $M = N = 5$ are now shown.

$$\begin{aligned} T(\zeta, \theta) = \zeta\{&1+\varepsilon(1-\zeta)+\varepsilon^2[(1-\zeta)^2+Q(1-\zeta)/2] \\ &+\varepsilon^3[(1-\zeta)^3+Q(1-\zeta)(1-2\zeta)/6] \\ &+\varepsilon^4[(1-\zeta)^4+Q(1-\zeta)^2(1-2\zeta)/6 \\ &+Gr\,Pr\cos\theta(1-5\zeta^3+6\zeta^4-2\zeta^5)/720] \\ &+\varepsilon^5[(1-\zeta)^5+Q(1-\zeta)^3(1-2\zeta)/6 \\ &+Gr\,Pr\cos\theta(43-35\zeta-455\zeta^3) \\ &+1057\zeta^4-840\zeta^5+230\zeta^6)/25{,}200] \\ &+O(\varepsilon^6)\} \end{aligned} \tag{13}$$

and

$$\begin{aligned} \psi(\zeta, \theta) = \sqrt{Gr}\sin^2\theta\zeta^2\{&-\varepsilon^3(1-\zeta)^2/24 \\ &+\varepsilon^4(2-3\zeta+\zeta^3)/120+\varepsilon^5[2(4-5\zeta-5\zeta^2 \\ &+9\zeta^3-3\zeta^4)-3Q(1-\zeta)^2(1-2\zeta)]/720+O(\varepsilon^6)\}. \end{aligned} \tag{14}$$

There are several comments necessarily made regarding the functions (13) and (14). First, the functions multiplied by ε^0 represent the associated thermal diffusion problem for a material contained between two parallel planes (in the Cartesian coordinate system) subject to (0, 1) boundary conditions. That is, for very small values of ε, the momentum equation reduces to $\psi \equiv 0$ and the Laplacian operator reverts to its Cartesian form. Secondly, notice that the conduction solution for the spherical annulus problem satisfying the same conditions is

$$T(r, \theta) = (r-\eta)/[r(1-\eta)], \tag{15}$$

or in terms of ζ and θ

$$T(\zeta, \theta) = \zeta[1-\varepsilon(1-\zeta)]^{-1}. \tag{16}$$

Since ζ is bounded by zero and one, and ε is a small, positive number, the quantity '$\varepsilon(1-\zeta)$' is also small so that (16) can be expanded in a binomial series giving, thus,

$$T(\zeta, \theta) = \zeta[1+\varepsilon(1-\zeta)+\varepsilon^2(1-\zeta)^2 + \varepsilon^3(1-\zeta)^3+\cdots]. \tag{17}$$

If (13) is forced to yield the conduction result only, by setting Gr and Q to zero, the exact series given by (17) is, not unexpectedly, reproduced. In effect, the perturbation solution is attempting to reproduce, to ever increasing accuracy, the solution for the spherical Laplacian operator. Finally, by examining the functions (13) and (14) it is found that internal energy generation effects are of higher order as are those of circulation on the temperature field (i.e. $\psi \neq 0$).

3.3. *Guidelines for the parameter values*

The solutions described above are found to be functions of the dimensionless parameters Gr, Pr, Q, and ε. These are available for manipulation, but not at will. By examining (13) and (14), it is noted that the various terms of the solutions containing the four parameters above could become large, certainly greater than one, causing a given nth-order solution to be larger than the $(n-1)$th-order solution. This implies a lack of convergence of the series. It is then necessary to establish some guidelines for parameter values.

The following two ratios involving all four dimensionless parameters of the problem suggest limits for their values. They are extracted from (13) and are such that they insure decreasing magnitudes of successive orders of solution. Thus, set

$$\frac{\varepsilon^2 Q}{2} < 1$$

and

$$\frac{\varepsilon^4 Gr\, Pr}{720} < 1. \tag{18}$$

It is suggested, then, that

$$Gr_{\text{lim}} = 720/\varepsilon^4 Pr \tag{19}$$

or

$$Pr_{\text{lim}} = 720/\varepsilon^4 Gr \tag{20}$$

and, for the generation rate function, Q

$$Q_{\text{lim}} = 2/\varepsilon^2. \tag{21}$$

As an example, suppose the geometry is selected so that $\varepsilon = 0.05$. Then

$$Q < Q_{\text{lim}} = 800$$

and

$$Gr < Gr_{\text{lim}} = 1.15 \times 10^8/Pr.$$

Since the guidelines result from the solution for $T(\zeta, \theta)$ it is necessary to examine their influence on $\psi(\zeta, \theta)$. Clearly, the magnitude of ψ is uniquely related to Gr_{lim} since $\sqrt{Gr}$ multiplies the entire solution. Also, the effect of Q on ψ is seen from (14) to be of the order of $3Q\varepsilon^5/720$, or smaller. Thus, if Q_{lim} from (21) is substituted into this ratio, the coefficient is then $\varepsilon^3/240$, clearly less than one.

Convergence of the series was tested in detail in ref. [8], and will not be reproduced here. The flows for $Gr = 6.5 \times 10^{12}$, $Pr = 0.01$, $\varepsilon = 0.01$, and $Q = 0$ were computed for $N = M = 3$, 7, 9, and 11. The isotherm and streamfunction contours were plotted and compared. The results for $N = M = 3$ and 7, and for 7 and 9 both, when compared with each other, showed marked changes, with those changes of the second set being less (qualitatively) than those of the first. Between $N = M = 9$ and 11, only minor or fine adjustments were observed in the flow field. This suggests that T and ψ have nearly converged for $N = M = 11$ in this case.

4. PRESENTATION OF RESULTS

The flow field is known in terms of the stream and temperature functions through $M = N = 11$ as outlined in Section 3 as

$$\psi, T = \psi, T(\zeta, \theta; Gr, Pr, Q, \varepsilon). \tag{22}$$

These results are presented as contours of constant values of ψ and T in the ζ–θ plane, which is a rectangular domain. The transformation (2) changes the very narrow gaps to a uniform rectangle, independent of ε. This is extremely helpful in observing the flow's nature since for $\varepsilon = 0.01$, for example, the gap width is only 1% of the outer sphere's radius. This is too narrow a region to effectively view the flow lines. Thus, the transformation not only simplifies the solution technique needed, but also expands the flow field so that it can be studied.

One of the most significant properties of the flow is the rate at which heat is transported across each sphere's boundary. This effect is commonly given as the Nusselt number, Nu, or as is sometimes expressed k_{eff}/k. This is the effective value of the fluid's thermal conductivity due to convection and conduction to its actual conductivity. It is this characteristic of the flow that is studied first with ψ and T given later.

4.1. *The Nusselt number*

It is possible to think of two Nusselt numbers, one representing the average value over a sphere's surface of the heat flux across that surface, and the other being an expression of the local, latitudinally varying surface flux. That is,

$$q^*(\theta) = -k\,\partial T^*/\partial r^*|_{R_i, R_o}. \tag{23}$$

This can be rewritten as

$$q^*(\theta) = -(k\Delta T/R_o\varepsilon)(\partial T/\partial\zeta)|_{0,1}. \tag{24}$$

Substituting the conduction temperature solution, excluding generation effects, into (24) gives

$$q_c^* = (-k\Delta T/R_o\varepsilon)(1-\varepsilon)[1-\varepsilon(1-\zeta)]^{-2}|_{0,1}. \tag{25}$$

The local Nusselt number, $Nu(\theta)$, is then

$$Nu(\theta) \equiv q^*/q_c^* = [(1-\varepsilon(1-\zeta))^2/(1-\varepsilon)](\partial T/\partial\zeta)|_{0,1}. \tag{26}$$

The average of $Nu(\theta)$, $\overline{Nu}$, is defined as

$$\overline{Nu} = \frac{\int_0^\pi q^*(\theta)\sin\theta\,d\theta}{\int_0^\pi q_c^*\sin\theta\,d\theta} = \frac{[1-\varepsilon(1-\zeta)]^2}{2(1-\varepsilon)}\int_0^\pi (\partial T/\partial\zeta)\sin\theta\,d\theta\Big|_{0,1}, \tag{27}$$

where $\overline{Nu} = \overline{Nu}(Gr, Pr, \varepsilon, Q)$. In the absence of internal energy sources or sinks, $\overline{Nu}$ must be the same value for a given Gr, Pr, and ε on each boundary so that selecting either $\zeta = 0$ or 1 is immaterial. Illustrations showing $Nu(\theta)$ are not given here, however, complete details are given in ref. [8].

Of interest are the data for $\overline{Nu}$. These are shown in Fig. 1 for $Q = 0$, $0.001 \leqslant \varepsilon \leqslant 0.1$, and $0.01 \leqslant Pr \leqslant 1000$. A new parameter, the Rayleigh number Ra', is used as the independent parameter since the data for the broad ranges of ε and Pr indicated collapse onto a single curve with maximum deviation of the data from the line being 0.15% with a standard deviation of 0.03%. Ra' is defined as

$$Ra' \equiv Gr\,Pr\,\varepsilon^4/\sqrt{1-\varepsilon}. \tag{28}$$

In refs. [9–11], Astill, and Leong *et al.* defined three regions of the flow field characterized by a predominantly conductive domain, a predominantly convective domain, and a transition domain connecting the prior two. The explicit definitions are:

Regime I: conduction

$$Nu \leqslant 1.001 \quad \text{or} \quad Ra' \leqslant 50$$

Regime II: transition

$$1.001 < \overline{Nu} < 1.12 \quad \text{or} \quad 50 < Ra' < 575 \tag{29}$$

Regime III: convection

$$\overline{Nu} \geqslant 1.12 \quad \text{or} \quad Ra' \geqslant 575.$$

Figure 2 compares these results with two other sets of data. In ref. [12], Brown was the first to compute large Rayleigh number flows in this geometry using finite difference methods. His data are not restricted to narrow gaps, but several runs were made for $\eta = 0.91$ (or $\varepsilon = 0.09$). Astill [9] also used a finite-difference method to compute flows for a variety of parameters including $\eta = 0.91$ and 0.97 (or $\varepsilon = 0.09$ and 0.03). Brown used a modified Rayleigh number, $Ra^+ = Gr\,Pr\,\varepsilon^4/(1-\varepsilon)$, which is a factor of $1/\sqrt{1-\varepsilon}$ larger than Ra', to develop a correlation for $\overline{Nu} = \overline{Nu}(Ra^+)$ as

$$\overline{Nu} = 0.186(Ra^+)^{0.269} \quad \text{for} \quad 0.09 \leqslant \varepsilon \leqslant 0.29 \tag{30}$$

with a standard deviation of 3.7%. Using Brown's data

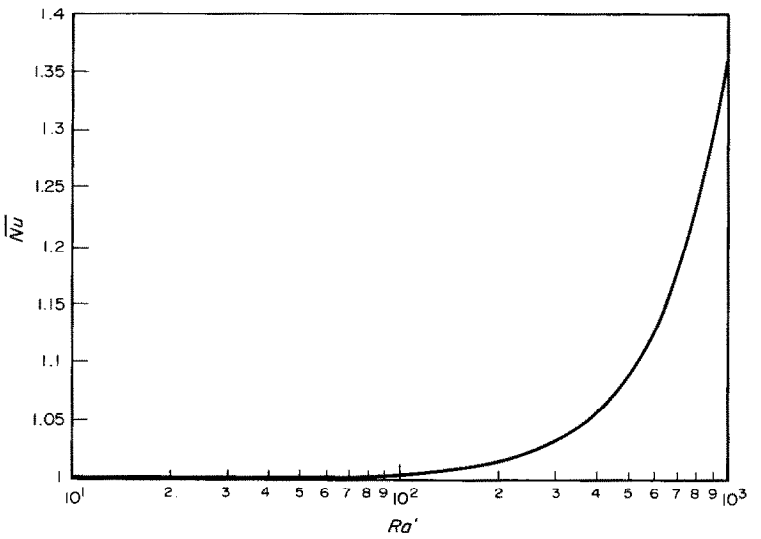

FIG. 1. The surface-averaged Nusselt number expressed as a function of the modified Rayleigh number, Ra'. This curve is a correlation of a series of results for $0.001 \leqslant \varepsilon \leqslant 0.1$ and $0.01 \leqslant Pr \leqslant 1000$. The curve has a maximum error of 0.15% and a standard deviation of 0.03%.

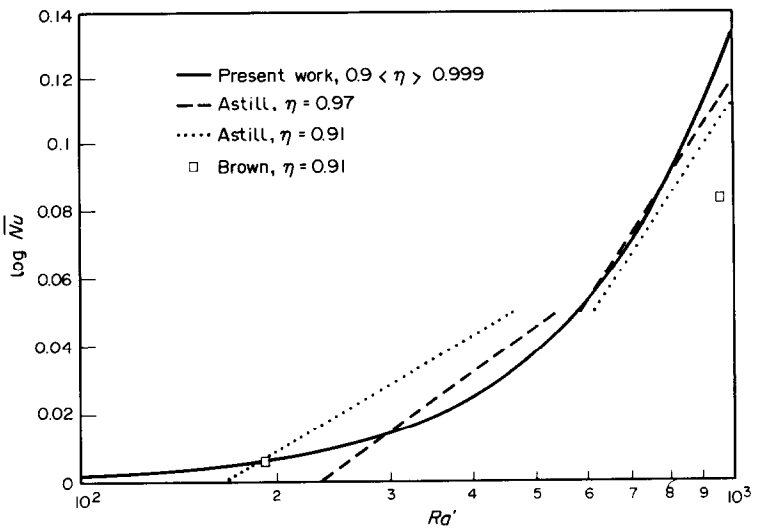

FIG. 2. A comparison of the current data for the Nusselt number with prior results. Note that $\eta = 1-\varepsilon$.

and refitting them to a correlation in terms of Ra' gives

$$\overline{Nu} = 0.184(Ra')^{0.275} \quad (31)$$

with a standard deviation of 1.6%, a somewhat better data fit. From the current results for small ε, correlations can be found giving

$$\overline{Nu} = 0.650(Ra')^{0.0824} \quad \text{for} \quad 50 < Ra' < 575 \quad (32)$$

and

$$\overline{Nu} = 0.116(Ra')^{0.355} \quad \text{for} \quad Ra' \geqslant 575, \quad (33)$$

where (32) has a standard deviation of 0.88% and (33) has 0.85% standard deviation.

4.2. *The flow field with* Q = 0

In this section, the influence on ψ and T of the parameters Gr, Pr, and ε are studied. The effect of energy sources are not a part of this section's discussion, but are studied in Section 4.3. Here, each parameter's influence is studied in turn by fixing two of them, while the third is allowed to vary. The guidelines of Section 3.3 are followed.

4.2.1. *Grashof number study.* The following four figures show how the flow field appears for values of Gr that place the flows in each of the regimes listed earlier. In these illustrations $Pr = 1$, $\varepsilon = 0.01$ and $Q = 0$ with $Gr = 0.5 \times 10^{10}$, 4×10^{10}, 5.7×10^{10}, and 7.45×10^{10} (i.e. $Ra' = 50$, 400, 575, and 750). Figure 3 is for a value of Gr at the end of the conduction regime. Here, the isotherms are very nearly parallel lines—i.e. concentric spherical shells in the (r, θ) coordinate system—as expected for heat conduction. The streamfunction is non-zero showing that fluid buoyancy is a factor. As in all cases shown in this paper, the flow is upward along

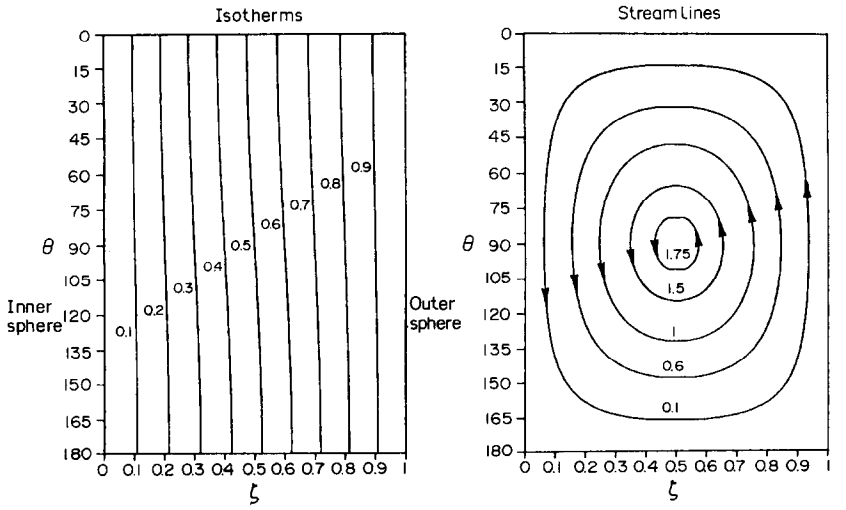

FIG. 3. The Grashof number series. In these flows $Pr = 1, \varepsilon = 0.01$ and $Q = 0$. Here $Gr = 0.5 \times 10^{10}$ (Ra' = 50). The streamline magnitudes have been multiplied by 10^4.

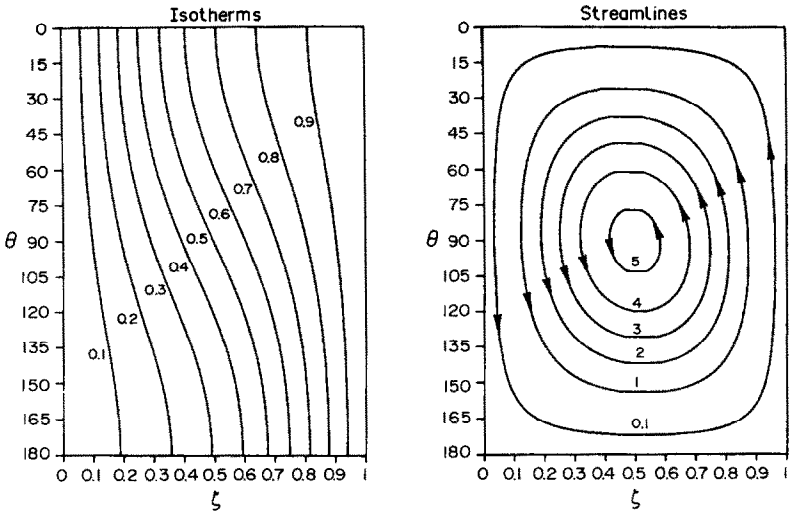

FIG. 4. The Grashof number series. In this case $Gr = 4 \times 10^{10}$ ($Ra' = 400$). The streamline magnitudes have been multiplied by 10^4.

the warm outer sphere and downward near the cool inner sphere. There is but one eddy, also characteristic of most of the flows shown here. Figure 4 is for a flow in the transition regime. Circulation of the fluid has an apparent effect on the fluid temperature since the relatively warm fluid has been convected towards the upper most part of the annulus, near $\theta = 0$ and ζ near 1, while the cool fluid has been moved to the lower part of the annulus ($\theta \simeq 180°, \zeta \simeq 0$). The peak circulation rate has increased by a factor of nearly three over those results in Figure 3. Figures 5 and 6 continue these trends with significant convective impact shown in Fig. 6. The isotherms are largely distorted, however, the streamlines are relatively undistorted with the peak circulation rate only a factor of 1.45 larger than in Fig. 4. These last results fall well within the Regime III domain.

Although no data are presented here, several computations were made for a reversal of the thermal boundary conditions. That is, let $T(\eta, \theta) = 1$ and $T(1, \theta) = 0$. This produces circulation patterns in the opposite sense compared with these data, but of the same absolute circulation rate for comparable parameter values. The isotherms were simply the mirror image of the results here. The Nusselt numbers were unchanged, as expected.

4.2.2. *Relative gap width study.* In this section, ε is allowed to vary while $Gr = 7 \times 10^6$, $Pr = 1.0$, and $Q = 0$. Figure 7 has a relatively wide gap width with $\varepsilon = 0.10$ (or $\eta = 0.9$) while Fig. 8 has $\varepsilon = 0.001$ (or $\eta = 0.999$), a very slim gap. In Fig. 8, the gap is so nar-

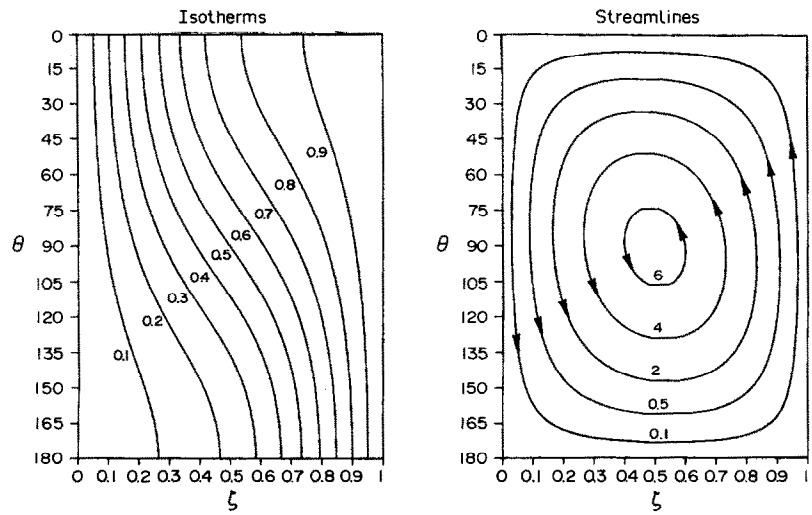

FIG. 5. The Grashof number series. In this case $Gr = 5.7 \times 10^{10}$ ($Ra' = 575$). The streamline magnitudes have been multiplied by 10^4.

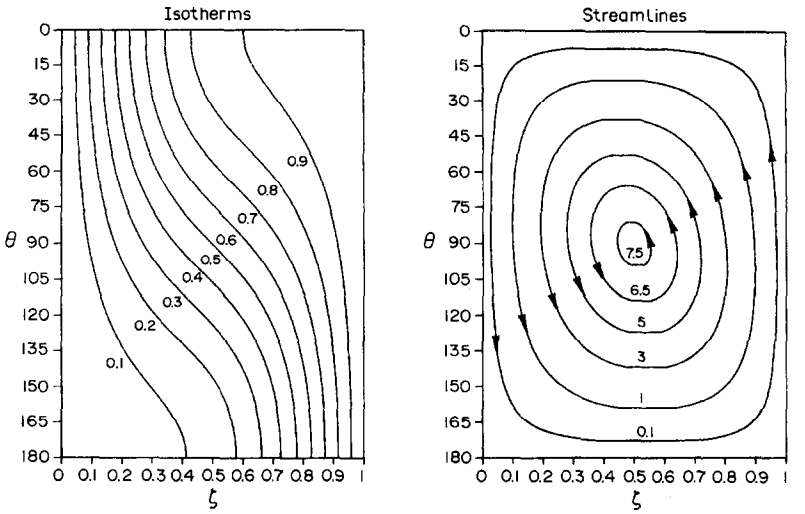

FIG. 6. The Grashof number series. In this case $Gr = 7.45 \times 10^{10}$ ($Ra' = 750$). The streamline magnitudes have been multiplied by 10^4.

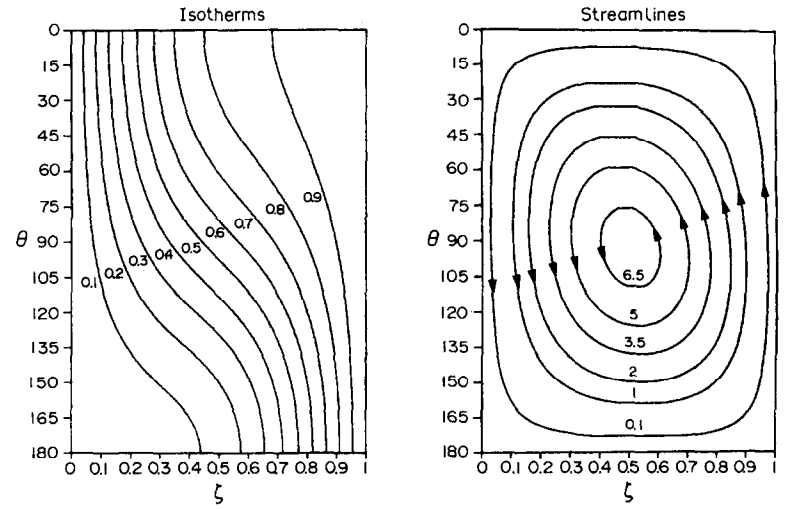

FIG. 7. The ε series. In these flows, $Gr = 7 \times 10^6$, $Pr = 1$, and $Q = 0$. Here $\varepsilon = 0.10$ ($Ra' = 738$). The streamline magnitudes have been multiplied by 10^3.

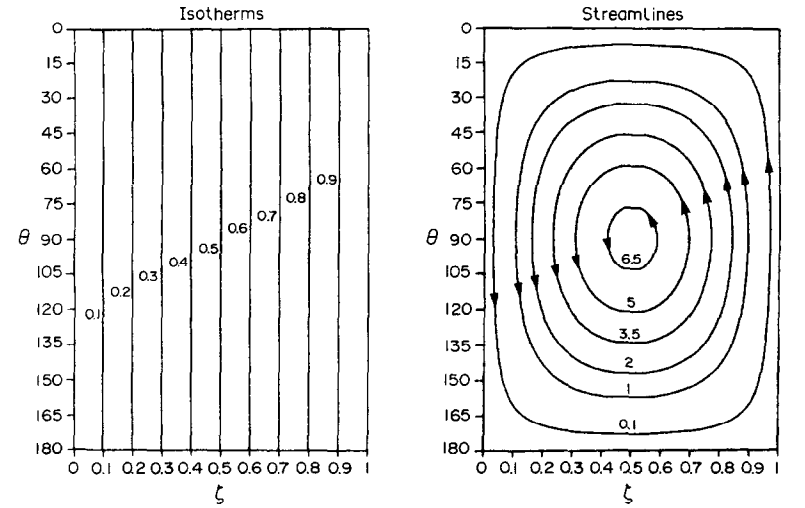

FIG. 8. The ε series. In this case $\varepsilon = 0.001$ ($Ra' = 7 \times 10^{-6}$). The streamline magnitudes have been multiplied by 10^9.

row as to virtually negate the effects of convection. The maximum value of ψ is -6.89×10^{-9} and the isotherms are essentially those for conduction. For the wider gap case the isotherms distort as in Fig. 6 and the maximum value of ψ increases to -7.04×10^{-3}. Comparing the values of maximum ψ shows that as ε increased by a factor of 10^2, the streamfunction increases by nearly a factor of 10^6. By examining (14) however, it is seen that for Gr, Pr, and Q fixed, the magnitude of ψ is proportional to ε^3, explaining this rather large variation in the magnitude of ψ. Note that in Fig. 8, $Ra' = 7 \times 10^{-6}$ while in Fig. 7, $Ra' = 738$. Thus, the $\varepsilon = 0.001$ case is very much as in Regime I and the $\varepsilon = 0.1$ case as in Regime III.

4.2.3. *Prandtl number study.* To illustrate the effect of Pr on the flow field, four values of Pr are selected covering three orders of magnitude: 0.01, 0.1, 1.0 and 10.0. Here, $Gr = 7 \times 10^9$, $\varepsilon = 0.01$, and $Q = 0$ and the results are shown in Figs. 9–12 for increasing values of Pr. In these cases, Ra' increases from 0.7 to 703.5, again covering all three flow regimes. By keeping Gr fixed, the kinematic viscosity (ν) is also fixed so that changing Pr implies changing the thermal diffusivity (α) so that $Pr = \nu/\alpha$ means that larger Pr are found for smaller values of α, and vice versa. Then, for small Pr, the fluid rapidly diffuses energy giving a conduction distribution. Likewise, for larger Pr, the fluid is not as able to diffuse energy, thereby retaining it longer. It is expected that as Pr increases, the more distorted the isotherms become indicating an increasing influence on the flow field of convection. These trends are borne out in the four figures of this section.

By again referring to the solution for T and ψ in algebraic form, Pr is first present in the ε^4-terms of the equation for T as shown in equation (13) while for ψ, it first appears in the ε^7-terms (cf. [8, p. 131]). Clearly the temperature is much more sensitive to Pr than the streamfunction. In fact, the streamline contours shown in Figure 9–12 are essentially identical with the maximum value of ψ very close to -2×10^{-4}.

4.3. *The flow field with energy sources*

As a final series of results, the effect on ψ and T of uniform volumetric energy sources within the fluid is examined. The presence of thermal sources causes the average temperature of the fluid to rise. Due to the annulus shape, it is expected that the fluid will attempt to arrange itself so that the warmest fluid will be found along the outer sphere and in the upper latitudes. Figure 13 and 14 demonstrate this trend. In these figures, $Gr = 8.95 \times 10^{10}$, $\varepsilon = 0.01$, $Pr = 1.0$, and $Q = 5000$ and 25,000, respectively. Data for a similar flow, but with $Q = 0$, are shown in Fig. 6. The shape of the circulation patterns is largely unaffected by Q, a surprising result at first thought. However, equation (14) for ψ shows that Q enters in the ε^5-term and is also multiplied by 3/720. It is, therefore, really not surprising that ψ is so insentitive to Q. The results for the distribution of $T(\zeta, \theta)$ are dramatically altered by Q. Equation (13) shows that Q effects T in the ε^2-terms.

The isotherms form two segregated regions in both figures; one with $T > 1$ and the other with $T < 1$. Those isotherms with $T < 1$ have a comparable shape for each Q, showing some distortion from the conduction profile. As Q grows, so does the region with $T > 1$, beginning as a nearly indistinguishable region in Fig. 13, but occupying roughly a quarter of the annulus in Fig. 14.

4.4. *Multicellular flows*

During the course of computing the flow fields for small values of the Prandtl number, it was observed that it was possible for the streamline patterns to change from a single cell to a multiple cell pattern. It was possible to define a Grashof number, $Gr'_c = Gr_c\varepsilon^4/(1-\varepsilon)^{1/2}$ which defines the onset of multicel-

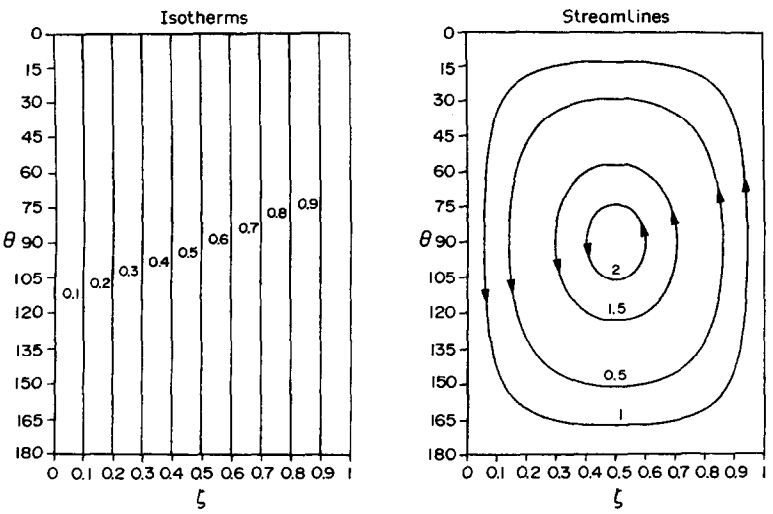

FIG. 9. The Prandtl number series. In these flows, $Gr = 7 \times 10^9$, $\varepsilon = 0.01$, and $Q = 0$. In this case $Pr = 0.01$ ($Ra' = 0.703$) and the streamline magnitudes have been multiplied by 10^4.

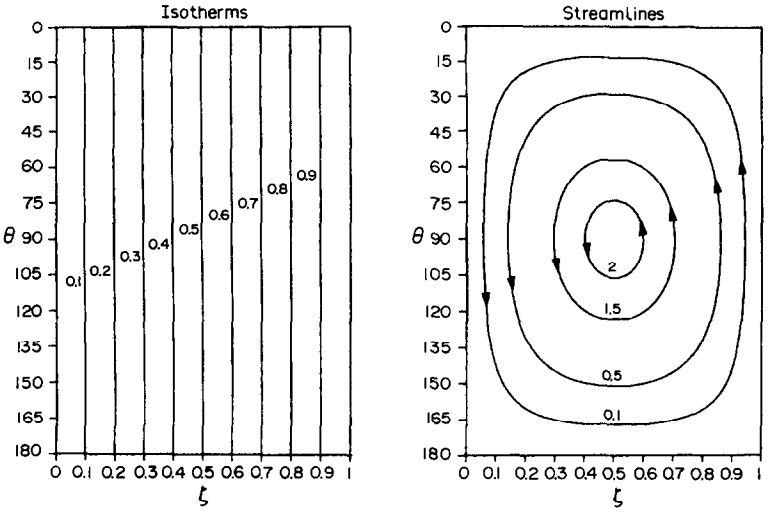

FIG. 10. The Prandtl number series. In these flows $Pr = 0.1$ ($Ra' = 7.03$) and the streamline magnitudes have been multiplied by 10^4.

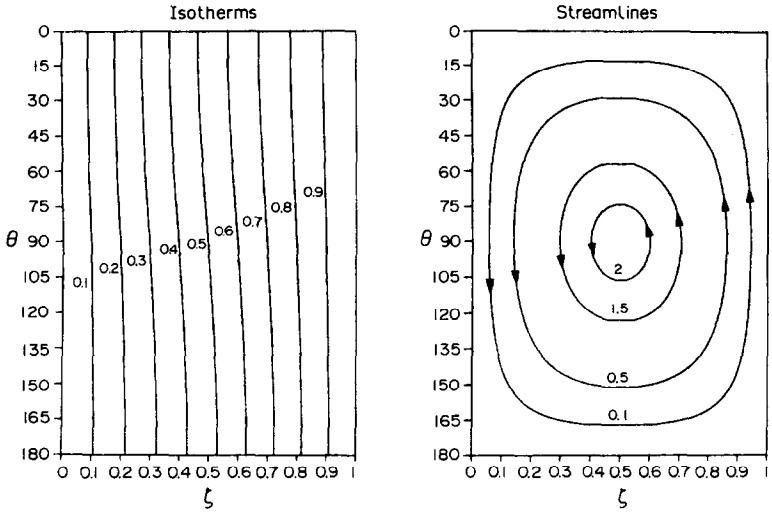

FIG. 11. The Prandtl number series. In these flows $Pr = 1.0$ ($Ra' = 70.3$) and the streamline magnitudes have been multiplied by 10^4.

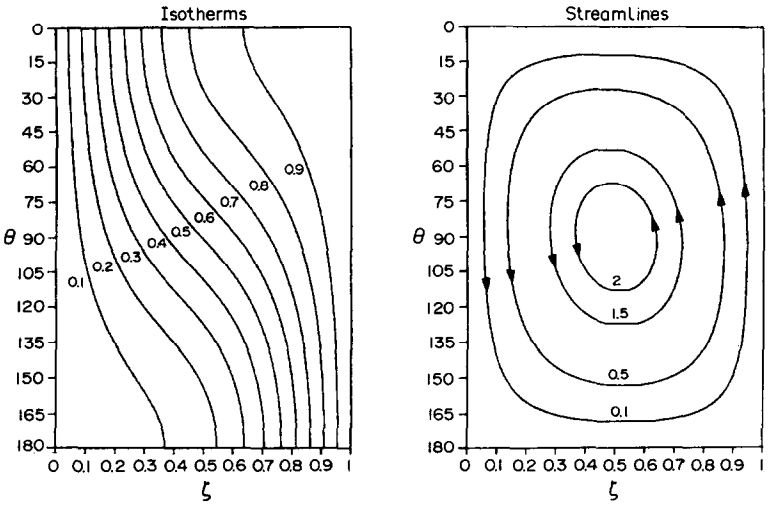

FIG. 12. The Prandtl number series. In these flows $Pr = 10.0$ ($Ra' = 703$) and the streamline magnitudes have been multiplied by 10^4.

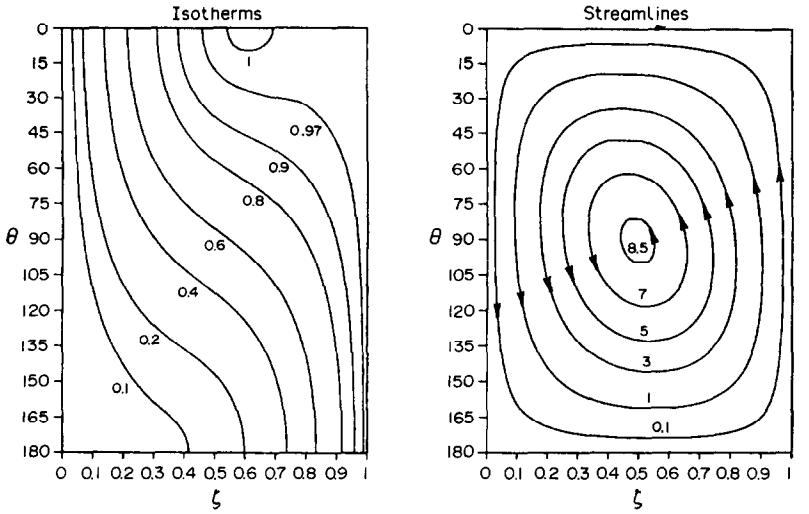

FIG. 13. The generation rate series. In these flows, $Gr = 8.95 \times 10^{10}$, $\varepsilon = 0.01$, and $Pr = 1.0 (Ra' = 900)$. Here $Q = 5000$ and the streamline magnitudes have been multiplied by 10^4.

lular flow. These results for $\eta = 0.9$ ($\varepsilon = 0.1$) and $\eta = 0.99$ ($\varepsilon = 0.01$) are shown in Fig. 15 which gives $Gr'_c = Gr'_c(Pr, \eta)$. Several features of these results are apparent. First, these critical values fall below the maximum Gr defined from the guidelines of equation (19) and so are valid results. Secondly, Gr' decreases as Pr increases for a given gap geometry. Thirdly, Gr'_c increases as the gap width narrows. Finally, no multicellular flows were found for Pr above one or, more positively, Pr values less than 0.2 were needed to produce multicellular flows.

A typical flow field demonstrating multiple eddy flow is shown in Fig. 16 for $Gr = 6.5 \times 10^{12}$, $\varepsilon = 0.01$, $Pr = 0.01$, and $Q = 0$. Here, the streamlines show two very large counter-rotating eddies located in the uppermost and lowermost parts of the annulus with the original single eddy highly distorted. The isotherm patterns are appropriately distorted by the convection pattern. The counter-rotating eddies carry some of the fluid adjacent to the boundaries towards the center of the annulus and also cause relatively warm and cool pockets of fluid near the upper and lower axes of the annulus, respectively.

The origin of the multiple cell circulation pattern can be explained as follows. It has been demonstrated that a small Pr value is necessary, but not sufficient, to form multiple cell flows. The joint requirement of large enough Gr' provides the closing concept. Thus, think of selecting a spherical geometry (R_i, R_o) and a fluid such that Pr is small enough (i.e. select β, ν, and α). Then, the only quantity left is the temperature difference, ΔT. Note that $\beta \Delta T$, within the Grashof number, is a measure

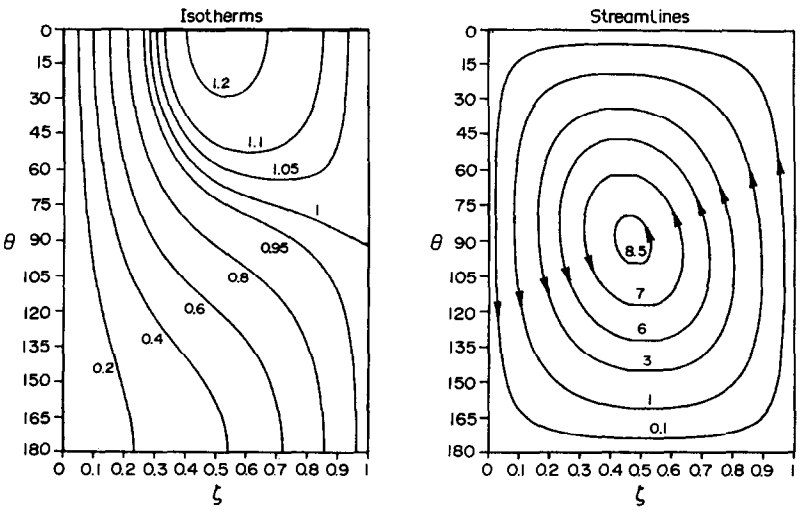

FIG. 14. The generation rate series. Here $Q = 25{,}000$ and the streamline magnitudes have been multiplied by 10^4.

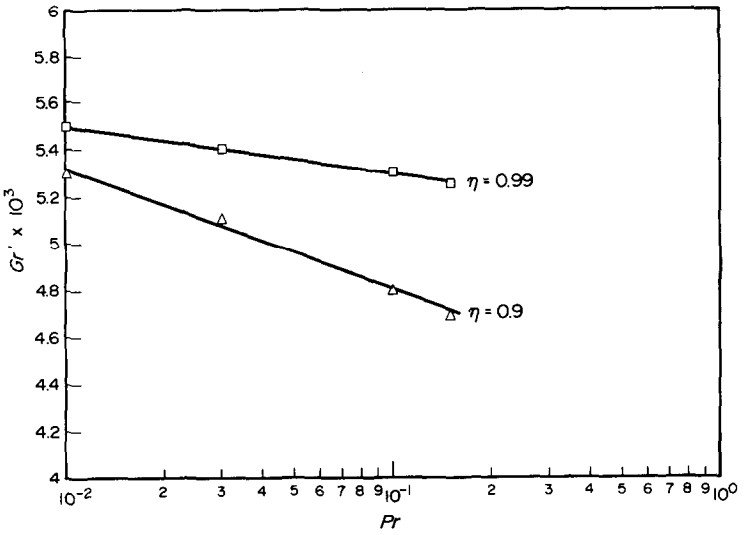

FIG. 15. Transition from unicellular to multiple cell flows. The ordinate is the value of $Gr' = Gr\,\varepsilon^4/\sqrt{\eta}$ which must be exceeded, for a given value of Pr, in order for the flow to change from unicellular to multicellular flow. In this sense, it is a critical value of Gr'. Note that $\eta = 1-\varepsilon$.

of local density variations due to temperature. Thus increasing the Grashof number is equivalent to increasing the sensitivity to buoyancy of the fluid. Using the isotherms together with the circulation patterns (e.g. Fig. 16) the reasoning proceeds as follows. With small Pr, the fluid readily adapts its temperature to its surroundings. Thus, the warmest (lightest) fluid will tend to seek the highest parts of the annulus and to remain there. A small eddy is spawned there for a value of Gr' just above the limiting value. This small eddy forces the bulk of the fluid to divert its path away from the outer boundary before it has completed its sweep over that boundary. By the time it is diverted, it is already essentially at the boundary temperature. The diverted fluid moves across the annulus towards the inner, cooler boundary where it comes into contact with it. Because of the small value of Pr, the fluid is rapidly cooled. As it is cooled, it becomes relatively heavy and ultimately drops away from the boundary. This also spawns an eddy trapped near the inner boundary in the lower latitudes. These small eddies grow as the buoyancy sensitivity increases (i.e. $\beta\Delta T$). The main eddy becomes more and more distorted as Gr' increases. These results suggest that the flow field ultimately will end up as four distinct eddies, for large enough Gr'.

5. CONCLUDING REMARKS

The research discussed in the prior four sections was done as a first step in the process of understanding the

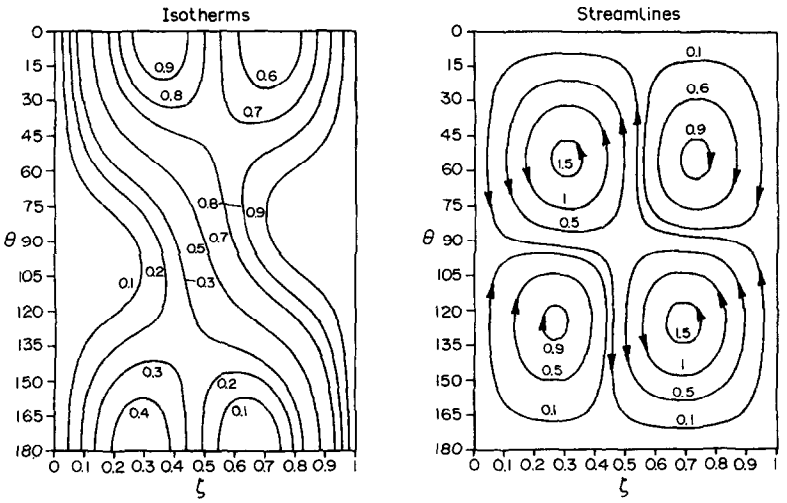

FIG. 16. An extreme example of multicellular flow for which $Gr = 6.5 \times 10^{12}$, $\varepsilon = 0.01$, $Pr = 0.01$, and $Q = 0$ ($Gr' = 6.5 \times 10^4$ or $Ra' = 650$). The streamline magnitudes have been multiplied by 10^2.

much larger problem of stability of natural convection in spherical annulus enclosures. The goal was to obtain a functional form of solution for this class of base flows which could be used in the stability and bifurcation analysis currently underway. A parallel goal was to understand the steady base flow itself. These have been successfully accomplished as detailed in the results presented.

It has been shown that for even a gap width of 0.1% of the outer sphere's radius, the fluid moves according to the general description of the steady flows given by Bishop *et al.* [2] and Yin *et al.* [4]. When in the unicellular regime, the convection occurs in the crescent eddy mode. The occurrence of multiple eddies here was for only small Pr fluids as compared with the results of refs. [2] and [4] for larger Pr values. These multiple eddies arise from the physics of the flow and are not associated with the hypothesized instability phenomenon.

Acknowledgements—The authors would like to express their thanks and appreciation to Mr Mitch Farmer who assisted in plotting the results shown herein, and to the Engineering Research Center of the College of Engineering and Technology of the University of Nebraska which supported this research.

REFERENCES

1. E. H. Bishop, Heat transfer by natural convection between isothermal concentric spheres, Ph.D. dissertation, University of Texas, Austin, TX (1964).
2. E. H. Bishop, L. R. Mack, and J. A. Scanlan, Heat transfer by natural convection between concentric spheres, *Int. J. Heat Mass Transfer* **9**, 649–662 (1966).
3. S. H. Yin, Natural convective flow between isothermal concentric spheres, Ph.D. dissertation, Montana State University, Bozeman, MT (1972).
4. S. H. Yin, R. E. Powe, J. A. Scanlan and E. H. Bishop, Natural convection flow patterns in spherical annuli, *Int. J. Heat Mass Transfer* **16**, 1785–1795 (1973).
5. R. E. Powe, R. O. Warrington and J. A. Scanlan, Natural convection between bodies and their spherical enclosures, 19th National Heat Transfer Conference. In *Heat Transfer in Enclosures*, HTD-Vol. 8 (Edited by K. E. Torrence and I. Catton). ASME, New York (1980).
6. R. E. Powe, R. O. Warrington and J. A. Scanlan, Natural convective flow between a body and its spherical enclosure, *Int. J. Heat Mass Transfer* **23**, 1337–1350 (1980).
7. D. Joseph, *Stability of Fluid Motion*, Vols I and II. Springer, New York (1980).
8. J. L. Wright, Natural convective flow in narrow gap spherical annuli, M.S. thesis, University of Nebraska, Lincoln, NB (1984).
9. K. N. Astill, Free convection between concentric spheres, Report No. R-1028, The Charles Stark Draper Laboratory, Inc., Cambridge, MA (1977).
10. H. T. Leong, Heat transfer between concentric spheres, M.S. thesis, Tufts University, Medford, MA (1979).
11. K. N. Astill, H. Leong and R. Martorana, A numerical solution for natural convection in concentric spherical annuli, 19th National Heat Transfer Conference. In *Heat Transfer in Enclosures*, HTD-Vol. 8. (Edited by K. E. Torrence and I. Catton). ASME, New York (1980).
12. R. J. Brown, Natural convection heat transfer between concentric spheres, Ph.D. dissertation, University of Texas, Austin, TX (1968).

APPENDIX: THE n-th ORDER GOVERNING EQUATIONS

Vorticity equation

$$\frac{\partial^4\psi_n}{\partial\zeta^4} = \left\{\left[5(1-\zeta)\frac{\partial^4}{\partial\zeta^4}\right]\psi_{n-1} + \left(\frac{Gr^{0.5}}{\sin\theta}\right)\sum_{i=0}^{n-1}\sum_{j=0}^{n-1}(\delta_{i+j,n-1})\left[(2\cot\theta)\left(\frac{\partial^2\psi_i}{\partial\zeta^2}\frac{\partial\psi_j}{\partial\zeta}\right)\right.\right.$$
$$\left.\left. + \left(\frac{\partial^3\psi_i}{\partial\zeta^3}\frac{\partial\psi_j}{\partial\theta} - \frac{\partial^3\psi_i}{\partial\zeta^2\,\partial\theta}\frac{\partial\psi_j}{\partial\zeta}\right)\right]\right\} + \left\{\left[10(1-\zeta)^2\frac{\partial^4}{\partial\zeta^4} - 2\left(\frac{\partial^4}{\partial\zeta^2\,\partial\theta^2} - (\cot\theta)\frac{\partial^3}{\partial\zeta^2\,\partial\theta}\right)\right]\psi_{n-2}\right.$$
$$\left. + \left(\frac{Gr^{0.5}}{\sin\theta}\right)\sum_{i=0}^{n-2}\sum_{j=0}^{n-2}(\delta_{i+j,n-2})\left[6(\zeta-1)(\cot\theta)\left(\frac{\partial^2\psi_i}{\partial\zeta^2}\frac{\partial\psi_j}{\partial\zeta}\right) - 2\left(\frac{\partial^2\psi_i}{\partial\zeta^2}\frac{\partial\psi_j}{\partial\theta}\right) + 3(\zeta-1)\left(\frac{\partial^3\psi_i}{\partial\zeta^3}\frac{\partial\psi_j}{\partial\theta} - \frac{\partial^3\psi_i}{\partial\zeta^2\,\partial\theta}\frac{\partial\psi_j}{\partial\zeta}\right)\right]\right\}$$
$$+ \left\{\left[6(1-\zeta)\left(\frac{\partial^4}{\partial\zeta^2\,\partial\theta^2} - (\cot\theta)\frac{\partial^3}{\partial\zeta^2\,\partial\theta}\right) + 10(1-\zeta)^3\frac{\partial^4}{\partial\zeta^4} + 4\left(\frac{\partial^3}{\partial\zeta\,\partial\theta^2} - (\cot\theta)\frac{\partial^2}{\partial\zeta\,\partial\theta}\right)\right]\psi_{n-3}\right.$$
$$- \left[Gr^{0.5}(\sin\theta)^2\frac{\partial}{\partial\zeta}\right]T_{n-3} + \left(\frac{Gr^{0.5}}{\sin\theta}\right)\sum_{i=0}^{n-3}\sum_{j=0}^{n-3}(\delta_{i+j,n-3})\left[6(\zeta-1)^2(\cot\theta)\left(\frac{\partial^2\psi_i}{\partial\zeta^2}\frac{\partial\psi_j}{\partial\zeta}\right)\right.$$
$$+ 3(\zeta-1)^2\left(\frac{\partial^3\psi_i}{\partial\zeta^3}\frac{\partial\psi_j}{\partial\theta} - \frac{\partial^3\psi_i}{\partial\zeta^2\,\partial\theta}\frac{\partial\psi_j}{\partial\zeta}\right) + (2\cot\theta)\left(\frac{\partial^2\psi_i}{\partial\theta^2} - (\cot\theta)\frac{\partial\psi_i}{\partial\theta}\right)\left(\frac{\partial\psi_j}{\partial\zeta}\right) + \left(\frac{\partial^3\psi_i}{\partial\zeta\,\partial\theta^2} - (\cot\theta)\frac{\partial^2\psi_i}{\partial\zeta\,\partial\theta}\right)\left(\frac{\partial\psi_j}{\partial\theta}\right)$$
$$\left.\left. - \left(\frac{\partial^3\psi_i}{\partial\theta^3} - \frac{\partial}{\partial\theta}\left((\cot\theta)\frac{\partial\psi_i}{\partial\theta}\right)\right)\left(\frac{\partial\psi_j}{\partial\zeta}\right) + 4(1-\zeta)\left(\frac{\partial^2\psi_i}{\partial\zeta^2}\frac{\partial\psi_j}{\partial\theta}\right)\right]\right\} + \left\{\left[5(1-\zeta)^4\frac{\partial^4}{\partial\zeta^4} + 6(1-\zeta)^2\left(\frac{\partial^4}{\partial\zeta^2\,\partial\theta^2} - (\cot\theta)\frac{\partial^3}{\partial\zeta^2\,\partial\theta}\right)\right.\right.$$
$$\left.\left. + 8(\zeta-1)\left(\frac{\partial^3}{\partial\zeta\,\partial\theta^2} - (\cot\theta)\frac{\partial^2}{\partial\zeta\,\partial\theta}\right) - \left(\frac{\partial^4}{\partial\theta^4} - 2(\cot\theta)\frac{\partial^3}{\partial\theta^3} + (5+3\,\mathrm{cosec}^2\,\theta)\frac{\partial^2}{\partial\theta^2} - 3(\cot\theta)(2+\mathrm{cosec}^2\,\theta)\frac{\partial}{\partial\theta}\right)\right]\psi_{n-4}\right.$$
$$+ Gr^{0.5}\left[6(1-\zeta)(\sin^2\theta)\frac{\partial}{\partial\zeta} - (\sin\theta)(\cos\theta)\frac{\partial}{\partial\theta}\right]T_{n-4} + \left(\frac{Gr^{0.5}}{\sin\theta}\right)\sum_{i=0}^{n-4}\sum_{j=0}^{n-4}(\delta_{i+j,n-4})\left[2(\zeta-1)^3(\cot\theta)\left(\frac{\partial^2\psi_i}{\partial\zeta^2}\frac{\partial\psi_j}{\partial\zeta}\right)\right.$$
$$+ (\zeta-1)^3\left(\frac{\partial^3\psi_i}{\partial\zeta^3}\frac{\partial\psi_j}{\partial\theta} - \frac{\partial^3\psi_i}{\partial\zeta^2\,\partial\theta}\frac{\partial\psi_j}{\partial\zeta}\right) + 2(1-\zeta)^2\left(\frac{\partial^2\psi_i}{\partial\zeta^2}\frac{\partial\psi_j}{\partial\theta}\right) + (1-\zeta)\left(\frac{\partial^3\psi_i}{\partial\theta^3} - \frac{\partial}{\partial\theta}\left((\cot\theta)\frac{\partial\psi_i}{\partial\theta}\right)\right)\left(\frac{\partial\psi_j}{\partial\zeta}\right)$$

$$+2(\zeta-1)(\cot\theta)\left(\frac{\partial^2\psi_i}{\partial\theta^2}-(\cot\theta)\frac{\partial\psi_i}{\partial\theta}\right)\left(\frac{\partial\psi_j}{\partial\zeta}\right)+(\zeta-1)\left(\frac{\partial^3\psi_i}{\partial\zeta\,\partial\theta^2}-(\cot\theta)\frac{\partial^2\psi_i}{\partial\zeta\,\partial\theta}\right)\left(\frac{\partial\psi_j}{\partial\theta}\right)-4\left(\frac{\partial^2\psi_i}{\partial\theta^2}-(\cot\theta)\frac{\partial\psi_i}{\partial\theta}\right)\left(\frac{\partial\psi_j}{\partial\theta}\right)\Bigg]\Bigg\}$$

$$+\Bigg\{\Bigg[(1-\zeta)^5\frac{\partial^4}{\partial\zeta^4}+2(1-\zeta)^3\left(\frac{\partial^4}{\partial\zeta^2\,\partial\theta^2}-(\cot\theta)\frac{\partial^3}{\partial\zeta^2\,\partial\theta}\right)+(1-\zeta)\left(\frac{\partial^4}{\partial\theta^4}-2(\cot\theta)\frac{\partial^3}{\partial\theta^3}+(5+3\,\mathrm{cosec}^2\,\theta)\frac{\partial^2}{\partial\theta^2}\right.$$

$$\left.-3(\cot\theta)(2+\mathrm{cosec}^2\,\theta)\frac{\partial}{\partial\theta}\right)+4(\zeta-1)^2\left(\frac{\partial^3}{\partial\zeta\,\partial\theta^2}-(\cot\theta)\frac{\partial^2}{\partial\zeta\,\partial\theta}\right)\Bigg]\psi_{n-5}\Bigg\}$$

$$+Gr^{0.5}\Bigg\{\Bigg[15(1-\zeta)^2(\sin^2\theta)\frac{\partial}{\partial\zeta}+5(1-\zeta)(\sin\theta)(\cos\theta)\frac{\partial}{\partial\theta}\Bigg]T_{n-5}+\Bigg[20(1-\zeta)^3(\sin^2\theta)\frac{\partial}{\partial\zeta}+10(1-\zeta)^2(\sin\theta)(\cos\theta)\frac{\partial}{\partial\theta}\Bigg]T_{n-6}$$

$$+\Bigg[15(1-\zeta)^4(\sin^2\theta)\frac{\partial}{\partial\zeta}+10(1-\zeta)^3(\sin\theta)(\cos\theta)\frac{\partial}{\partial\theta}\Bigg]T_{n-7}+\Bigg[6(1-\zeta)^5(\sin^2\theta)\frac{\partial}{\partial\zeta}+5(1-\zeta)^4(\sin\theta)(\cos\theta)\frac{\partial}{\partial\theta}\Bigg]T_{n-8}$$

$$+\Bigg[(1-\zeta)^6(\sin^2\theta)\frac{\partial}{\partial\zeta}+(1-\zeta)^5(\sin\theta)(\cos\theta)\frac{\partial}{\partial\theta}\Bigg]T_{n-9}\Bigg\}.$$

Energy equation

$$\frac{\partial^2T_n}{\partial\zeta^2}=\Bigg[2(1-\zeta)\frac{\partial^2}{\partial\zeta^2}-(2)\frac{\partial}{\partial\zeta}\Bigg]T_{n-1}+\Bigg[(1-\zeta)^2\frac{\partial^2}{\partial\zeta^2}+2(1-\zeta)\frac{\partial}{\partial\zeta}-\frac{\partial^2}{\partial\theta^2}-(\cot\theta)\frac{\partial}{\partial\theta}\Bigg]T_{n-2}$$

$$+\left(\frac{Gr^{0.5}\,Pr}{\sin\theta}\right)\Bigg[\sum_{i=0}^{n-1}\sum_{j=0}^{n-1}(\delta_{i+j,n-1})\left(\frac{\partial T_i}{\partial\zeta}\frac{\partial\psi_j}{\partial\theta}-\frac{\partial T_i}{\partial\theta}\frac{\partial\psi_j}{\partial\zeta}\right)\Bigg]+[-\delta_{n,2}+2(1-\zeta)\delta_{n,3}+(1-\zeta)^2\delta_{n,4}]Q.$$

Boundary conditions

$$\frac{\partial\psi_n(0,\theta)}{\partial\zeta}=\frac{\partial\psi_n(0,\theta)}{\partial\theta}=\frac{\partial\psi_n(1,\theta)}{\partial\zeta}=\frac{\partial\psi_n(1,\theta)}{\partial\theta}=0$$

$$\frac{\partial\psi_n(\zeta,\theta)}{\partial\theta}=\frac{\partial\psi_n(\zeta,-\theta)}{\partial\theta},\frac{\partial\psi_n(\zeta,\theta)}{\partial\zeta}=\frac{\partial\psi_n(\zeta,-\theta)}{\partial\zeta},\frac{\partial\psi_n(\zeta,0)}{\partial\zeta}=\frac{\partial\psi_n(\zeta,\pi)}{\partial\zeta}=0$$

$$T_n(\zeta,\theta)=T_n(\zeta,-\theta),\frac{\partial T_n(\zeta,0)}{\partial\theta}=\frac{\partial T_n(\zeta,\pi)}{\partial\theta}=0$$

$$T_n(0,\theta)=0,\quad T_n(1,\theta)=\delta_{n0}.$$

CONVECTION NATURELLE DANS UN ESPACE ETROIT ENTRE SPHERES CONCENTRIQUES

Résumé—On considère la convection naturelle d'un fluide enfermé dans un espace étroit entre sphères concentriques. L'écoulement est supposé permanent et répondant au modèle Oberbeck–Boussinesq. L'espace étant mince devant le rayon de la sphère extérieure, les variables sont résolues en utilisant une méthode de perturbation en puissance de la largeur ε. Des solutions sont trouvées pour une sphère extérieure chaude, en termes jusqu'à ε^{11}. Les résultats incluent les nombres de Nusselt, les lignes de courant et les isothermes en fonction des nombres de Grashof et de Prandtl, de ε et de Q le paramètre adimensionnel uniforme de source d'énergie. La valeur de ε est comprise entre 0,1 et 0,001, celles de Pr entre 0,01 et 10, celles de Gr entre 7×10^6 et 5×10^{12}.

NATÜRLICHE KONVEKTION IN EINEM ENGEN KUGELFÖRMIGEN SPALT

Zusammenfassung—Der Gegenstand dieser Abhandlung ist die natürliche Konvektion in einem engen kugelförmigen Spalt. Es wird angenommen, daß die Strömung stationär ist, und das Fluid dem Oberbeck–Boussinesq Modell folgt. Für den Fall, daß die Spaltbreite im Verhältnis zum Durchmesser der äußeren Kugel sehr klein ist, werden die abhängigen Variablen mit Hilfe eines gewöhnlichen Störungsverfahrens als Potenzfunktion der relativen Spaltbreite ε ermittelt. Die Ergebnisse umfassen Nusselt-Zahlen, Stromlinien und Isothermen als Funktion der Grashof- und der Prandtl-Zahl, der relativen Spaltbreite und des dimensionslosen Parameters Q für den gleichmäßig übertragenen Wärmestrom. Die Werte für ε reichen von 0,1 bis 0,001, für Pr von 0,01 bis 10 und für Gr von 7×10^6 bis 5×10^{12}.

ЕСТЕСТВЕННАЯ КОНВЕКЦИЯ В ТОНКОМ СФЕРИЧЕСКОМ СЛОЕ

Аннотация—Изучалась естественная конвекция жидкости, находящейся в узком зазоре между концентрическими сферами. Течение считалось стационарным, была принята модель Обербека–Буссинеска. В случае, когда зазор очень мал по сравнению с радиусом внешней сферы, зависимые переменные находятся с помощью регулярного метода возмущений по степеням относительной толщины слоя ε. Для нагретой наружной сферы решения найдены вплоть до членов порядка ε^{11}. Получены зависимости чисел Нуссельта, изолиний тока и изотерм от чисел Грасгофа и Прандтля, величины ε и Q—безразмерного параметра, характеризующего мощность выделяющейся энергии. Величины ε варьировались в диапазоне от 0,1 до 0,001, Pr от 0,01 до 10 и Gr от 7×10^6 до 5×10^{12}.